JOURNAL OF VIROLOGY, Nov. 2004, p. 12603–12612 Vol. 78, No. 22
0022-538X/04/$08.00+0 DOI: 10.1128/JVI.78.22.12603–12612.2004

Enhanced Cellular Receptor Usage by a Bioselected Variant of Coxsackievirus A21

E. Susanne Johansson,[1]* Li Xing,[2] R. Holland Cheng,[2] and Darren R. Shafren[1,3]

Picornaviral Research Unit, Discipline of Immunology and Microbiology, Faculty of Medical Sciences, The University of Newcastle,[1] and ViroTarg Pty. Ltd.,[3] Newcastle, New South Wales, Australia, and Department of Biosciences, Karolinska Institute, Huddinge, Sweden[2]

Received 19 March 2004/Accepted 6 July 2004

Decay-accelerating factor (DAF) functions as cell attachment receptor for a wide range of human enteroviruses. The Kuykendall prototype strain of coxsackievirus A21 (CVA21) attaches to DAF but requires interactions with intercellular cell adhesion molecule 1 (ICAM-1) to infect cells. We show here that a bioselected variant of CVA21 (CVA21-DAFv) generated by multiple passages in DAF-expressing, ICAM-1-negative rhabdomyosarcoma (RD) cells acquired the capacity to induce rapid and complete lysis of ICAM-1-deficient cells while retaining the capacity to bind ICAM-1. CVA21-DAFv binding to DAF on RD cells mediated lytic infection and was inhibited by either antibody blockade with a specific anti-DAF SCR1 monoclonal antibody (MAb) or soluble human DAF. Despite being bioselected in RD cells, CVA21-DAFv was able to lytically infect an additional ICAM-1-negative cancer cell line via DAF interactions alone. The finding that radiolabeled CVA21-DAFv virions are less readily eluted from surface-expressed DAF than are parental CVA21 virions during a competitive epitope challenge by an anti-DAF SCR1 MAb suggests that interactions between CVA21-DAFv and DAF are of higher affinity than those of the parental strain. Nucleotide sequence analysis of the capsid-coding region of the CVA21-DAFv revealed the presence of two amino acid substitutions in capsid protein VP3 (R96H and E101A), possibly conferring the enhanced DAF-binding phenotype of CVA21-DAFv. These residues are predicted to be embedded at the interface of VP1, VP2, and VP3 and are postulated to enhance the affinity of DAF interaction occurring outside the capsid canyon. Taken together, the data clearly demonstrate an enhanced DAF-using phenotype and expanded receptor utilization of CVA21-DAFv compared to the parental strain, further highlighting that capsid interactions with DAF alone facilitate rapid multicycle lytic cell infection.

The attachment of viruses to cell surface molecules is the initial step of virus replication, and specific cellular virus receptors are therefore major determinants for virus tissue tropism. Decay-accelerating factor (DAF; CD55), a 70-kDa glycosylphosphatidylinositol-anchored complement-regulatory protein consisting of four extracellular short consensus repeats (SCRs) (25), serves as a membrane attachment protein for numerous human enteroviruses, including several echoviruses (EV) (4, 20, 36, 48), coxsackie B viruses (CVB) (41) and coxsackievirus A21 (CVA21) (43). In general, viral binding to DAF alone is insufficient to permit enteroviral infections and interactions with DAF do not induce 135S altered (A) particles (34, 35, 39, 43, 45), which are considered to be a prerequisite for cell entry (2, 50). The physiological role of DAF for enteroviral infections is postulated to be that of a membrane concentration receptor that binds and clusters the infectious virus, resulting in increased opportunity for cell entry via interactions with a second functional cell entry receptor (30, 43, 45).

As with many other picornaviruses (the polioviruses, the major-receptor group rhinoviruses, and CVBs) (3, 5, 10, 13, 15, 22), the CVA21 cellular internalizing receptor, intercellular cell adhesion molecule 1 (ICAM-1; CD54), is a member of the immunoglobulin superfamily and binds within the capsid canyon surrounding the fivefold axis (43, 49). Interactions between the viral receptor at the base of the canyon destabilize the capsid and induce conformational changes, a prelude to viral uncoating (1, 3, 12, 16).

The prototype strain of CVA21 (Kuykendall), a causal agent of respiratory infections (32), binds to both ICAM-1 and DAF. Binding of the prototype strain of CVA21 to surface-expressed DAF is not sufficient to initiate a productive infection or formation of A particles, with interaction with ICAM-1 required for cell entry (30, 43). However, when surface DAF is cross-linked via specific interactions with a monoclonal antibody (MAb) directed against a nonviral binding domain of DAF (i.e., SCR2-4), CVA21 lytic infection can occur in the absence of ICAM-1 (39). Recently, low-cell-culture-passage clinical isolates of CVA21 were shown to bind both DAF and ICAM-1, with the DAF-binding phenotype therefore not likely to be acquired from multiple passages in cell culture (31). Increasing evidence for a more active role of DAF in enteroviral infections is demonstrated by the enhanced DAF-using phenotype of such clinical CVA21 isolates, which, to various degrees, possess the capacity to lytically infect DAF-expressing cells in the absence of anti-DAF MAb cross-linking or surface-expressed ICAM-1 (31).

In the present study we investigated the specific nature of the receptor usage of a variant of CVA21 (CVA21-DAFv),

* Corresponding author. Mailing address: Picornaviral Research Unit, Discipline of Immunology and Microbiology, Faculty of Health, The University of Newcastle, Level 3, David Maddison Clinical Sciences, Bldg., 2300 Newcastle, New South Wales, Australia. Phone: 61 2 49236150. Fax: 61 2 49236814. E-mail: susanne.johansson@newcastle.edu.au.

bioselected to lytically infect ICAM-1-negative rhabdomyosarcoma (RD) cells. We show that after multiple passages in DAF-expressing RD cells, CVA21-DAFv exhibits an enhanced capacity to bind to DAF compared to the parental strain while retaining the potential to bind ICAM-1. Lytic infection of RD cells is completely abolished by an anti-DAF SCR1 MAb blockade, suggesting that interactions with DAF alone mediate lytic infection. Nucleotide sequence analysis of the capsid-coding region revealed the presence of two unique amino acid substitutions in VP3 of CVA21-DAFv predicted to confer enhanced viral capsid interactions with DAF.

MATERIALS AND METHODS

Cells and viruses. The human melanoma cell line SkMel28 was obtained from S. J. Ralph (Department of Biochemistry and Molecular Biology, Monish University, Victoria, Australia); RD cells were obtained from Margery Kennett (Entero-Respiratory Laboratory, Fairfield Hospital, Melbourne, Victoria, Australia); Chinese hamster ovary (CHO) cells were obtained from Bruce Loveland (Austin Research Institute, Heidelberg, Victoria, Australia); and the ovarian cancer cell line DOV13 was obtained from Ian Campbell (Peter MacCallum Cancer Centre, Melbourne, Australia). CHO cells stably expressing ICAM-1 or DAF (CHO-DAF and CHO-ICAM-1 cells) have been previously reported (29). Prototype strains of CVA20 (IH-35) and CVA21 (Kuykendall; GenBank accession number AF465515) were obtained from Margery Kennett and propagated in RD cells stably expressing ICAM-1 (29) and SkMel28 cells, respectively.

Antibodies. The anti-DAF MAb IH4, specific for SCR3 of DAF (11), was a gift from Bruce Loveland; anti-DAF MAb IA10 directed against SCR1 (21) was a gift from Taroh Kinoshita (Department of Immunoregulation, Osaka University, Osaka, Japan); and the anti-ICAM-1 WEHI MAb is directed against the N-terminal domain of ICAM-1 (8) and was supplied by Andrew Boyd (Queensland Institute for Medical Research, Queensland, Australia).

Flow cytometry. Dispersed cells (10^6) were incubated on ice with anti-DAF IH4 or anti-ICAM-1 MAb (5 μg/ml, diluted in phosphate-buffered saline [PBS]) for 20 min. The cells were then washed with PBS, pelleted at $1,000 \times g$ for 5 min, resuspended in 100 μl of the R-phycoerythrin-conjugated $F(ab')_2$ fragment of goat anti-mouse immunoglobulin diluted 1:100 in PBS (DAKO A/S, Copenhagen, Denmark), and incubated on ice for 20 min. The cells were washed and pelleted as above, resuspended in PBS, and analyzed for DAF and ICAM-1 expression by using a FACStar analyzer (Becton Dickenson, Sydney, Australia).

Virus infectivity assay. Confluent cell monolayers in 96-well plates were inoculated with 100 μl of 10-fold serial dilutions of virus and incubated at 37°C for 72 h. To quantitate cell survival, the plates were microscopically examined and then fixed with a crystal violet-methanol solution. Fifty percent endpoint titers were calculated using the method of Reed and Muench (37). For assessing anti-DAF SCR1 MAb blockade of virus-mediated cell lysis, RD monolayers in 96-well plates were incubated with 50 μl of MAb IA10 (5 μg/ml) for 1 h at 37°C prior to challenge with virus (10^6 50% tissue culture infective doses [$TCID_{50}$]). Following incubation for 24 h at 37°C, the cells were inspected for cell lysis by microscopic examination. To assess the effect of MAb cross-linking of DAF, cell monolayers in 96-well plates were preincubated with anti-SCR3 MAb IH4 (5 μg/ml) for 1 h at 37°C prior to the addition of virus and quantitation of cell lysis as above.

Radiolabeled virus binding assays. The parental and CVA21-DAFv strains were radiolabeled with [^{35}S]methionine in SkMel28 and RD cells, respectively, and purified on 5 to 30% sucrose gradients as previously described (29). Dispersed cells (10^6) were preincubated with MAbs (20 μg/ml diluted in Dulbecco's modified Eagle's medium [DMEM] containing 1% bovine serum albumin) for 1 h at room temperature and then incubated for 1 h at room temperature with ^{35}S-labeled sucrose-purified virus (5×10^5 cpm) in DMEM containing 2% fetal calf serum (FCS). Following three washes with DMEM–2% FCS, the amount of [^{35}S]methionine-labeled virus bound was measured by liquid scintillation counting on a 1450 Microbeta TRILUX (Wallac, Turku, Finland).

Elution of cell-bound virus by anti-DAF MAb. CHO-DAF cells (3×10^6) were incubated at 4°C for 2 h with radiolabeled virus (4×10^5 cpm). Unbound virions were removed by four washes with ice-cold DMEM–2% FCS, and the cells were resuspended in 100 μl of DMEM–2% FCS and incubated with different concentrations (0 to 50 μg/ml) of anti-DAF SCR1 MAb (IA10). Following MAb competition for 1 h on ice, the cells were pelleted and the supernatant was harvested. Cell pellets and supernatants were monitored for the level of eluted virus, and the results were expressed as the percentage of cell-eluted radiolabeled virus.

Sedimentation of DAF- and ICAM-1-bound virions. Purified radiolabeled 160S CVA21-DAFv virions (2.5×10^6 cpm) were incubated with CHO-DAF or CHO-ICAM-1 cells (2×10^7) in DMEM–1% bovine serum albumin for 2 h at 4°C. Unbound virions were removed by four washes with DMEM–2% FCS, and cell-bound virions were permitted to elute for 2 h at 37°C. The cells were removed by centrifugation, and the eluted virions were layered on 5 to 30% sucrose gradients and centrifuged for 95 min at 4°C in an SW41Ti rotor at 36,000 rpm. Fractions (~700 μl) were collected from the bottom of the gradient, and radioactivity was determined by liquid scintillation counting.

Neutralization of virus with soluble DAF. Human soluble DAF (sDAF cDNA cloned into the pAPEX-3P vector) was expressed in human 293-EBNA cells (B. Loveland and P. Kyriakou, unpublished data). Soluble DAF (1.2 μM, diluted in PBS) was incubated with 10^3 $TCID_{50}$ of CVA20 and CVA21-DAFv. Following incubation at 37°C for 1 h, the virus-DAF mixtures were applied to monolayers of RD cells in a 96-well plate and further incubated for 48 h and then inspected for cell lysis by microscopic examination.

Molecular characterization of viruses. Viral RNA was extracted from the CVA21 parental and CVA21-DAFv strains by using the QIAamp viral RNA mini kit, and the capsid-coding region was amplified by one-step reverse transcription-PCR (RT-PCR) (Qiagen OneStep RT-PCR kit) as specified by the manufacturer, using CVA21-specific primers (29). The nucleotide sequences were determined using purified PCR products (QIAquick gel extraction kit; QIAGEN GmbH) in a cycle-sequencing reaction using the ABI Prism BigDye terminator cycle-sequencing ready reaction kit (PE Biosystems) as specified by the manufacturer.

Structural modeling. The model of the CVA21 major structural proteins (VP1 to VP3) was built with the program Modeller in a DEC alpha-station, in a manner similar to that used for the prediction of the poliovirus receptor structure (38, 52). The CVA21 parental sequence was aligned against homologous enteroviral capsid proteins, for which the molecular structures have previously been determined and contain sequence identities above 50%, which include poliovirus 1, EV1, EV11, CVB3, CVA9, and swine vesicular disease virus (PDB code 1AR7, 1EV1, 1H8T, 1COV, 1D4M, and 1OOP, respectively), with alignment created by FASTA (33). The positions of ICAM-1 and DAF with respect to the CVA21-DAFv capsid were aligned according to their ligand contact with human rhinovirus 3 and EV12, respectively (7, 50).

RESULTS

Bioselection of a CVA21 variant that lytically infects cells independently of ICAM-1 interactions. Cellular attachment of the CVA21 prototype strain is mediated by binding to DAF and/or ICAM-1. Only ICAM-1 interactions facilitate cell entry (43), while interactions between the CVA21 prototype and DAF do not induce productive lytic cell infection unless DAF is cross-linked by anti-DAF MAbs (39). CVA21 can lytically infect DAF-expressing RD cells when the cells are transfected with ICAM-1 (43), highlighting the fact that the inability of CVA21 to replicate in RD cells is at the level of cell entry. The human melanoma cell line SkMel28 supports growth of the prototype strain of CVA21 to high viral titers (40), and flow cytometric analysis revealed, as expected, high levels of both ICAM-1 (geometric mean fluorescence [GMF] = 57.2) and DAF (GMF = 43.2) surface expression (Fig. 1A).

A preparation of the CVA21 prototype strain, double-plaque purified in SkMel28 cells (herein designated CVA21 parental), was adapted to produce a rapid lytic infection of RD cells by repeated passages (five sequential passages). Flow cytometric analysis revealed that RD cells express a comparable level of DAF (GMF = 64.0) to that in SkMel28 cells (Fig. 1A). No expression of ICAM-1 was detected on RD cells, and we have previously shown that no ICAM-1 mRNA can be detected in RD cells (39). Sequential passage of the parental CVA21 in RD cells bioselected for a CVA21 variant (designated CVA21-DAFv) from the parental population that pos-

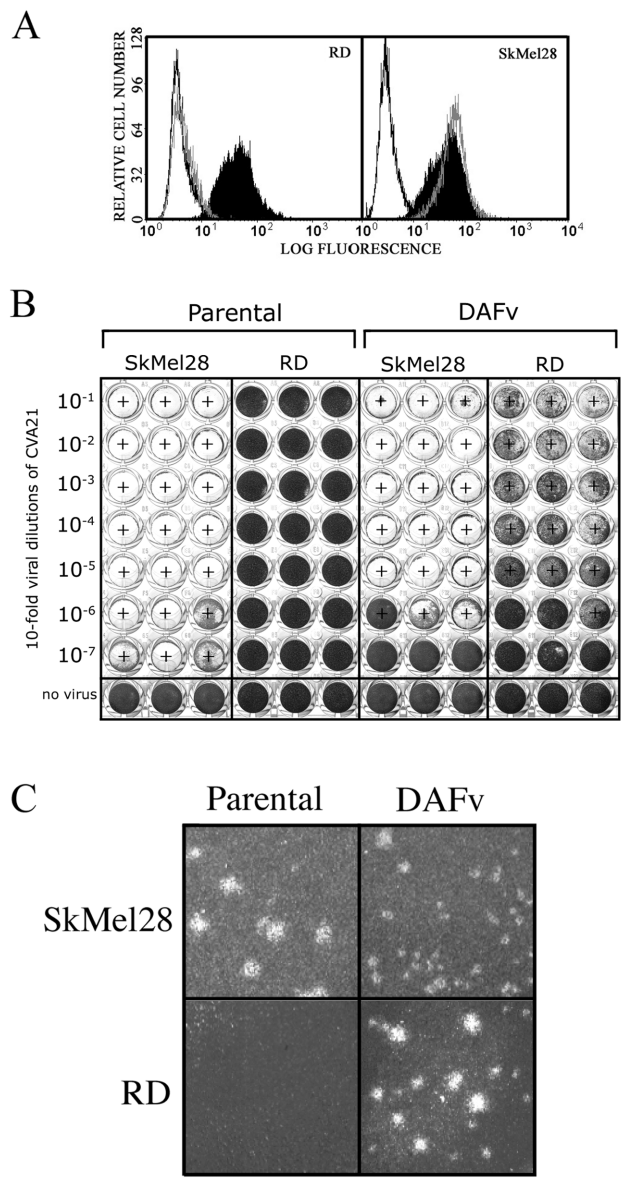

FIG. 1. Infection of SkMel28 and RD cells by CVA21 parental and CVA21-DAFv. (A) Flow cytometric analysis of ICAM-1 and DAF expression on RD and SkMel28 cells. The open histogram represents binding of conjugate only; the dotted histogram represents binding of anti-ICAM-1 MAb; and the solid histogram represents binding of anti-DAF MAb. (B) Monolayers of SkMel28 and RD cells in 96-well plates were inoculated with 10-fold dilutions of stock preparations of parental CVA21 and CVA21-DAFv. Following incubation for 72 h at 37°C, the monolayers were fixed and stained with a crystal violet solution. Plus signs indicate that a cytopathic effect was detected by microscopic examination. (C) Representative plaque morphology of the parental CVA21 and CVA21-DAFv on SkMel28 cells compared with the CVA21-DAF variant on RD cells. Cell monolayers in six-well plates were infected with virus and overlaid with DMEM–0.7% agarose 1 h after infection. Following a 48-h incubation at 37°C, the plates were stained with crystal violet.

sessed the capacity to induce rapid lytic infection in the absence of ICAM-1 (Fig. 1B). Dual ICAM-1- and DAF-expressing SkMel28 cells supported lytic infection of both the parental CVA21 and CVA21-DAFv at titers at excess of 10^7 $TCID_{50}$/ml, while only CVA21-DAFv induced a comparable lytic titer in RD cells (Fig. 1B).

Phenotypic properties of CVA21-DAFv. Following adaptation to ICAM-1-negative RD cells, CVA21-DAFv produced plaques with similar efficiency on monolayers of both SkMel28 and RD cells (5×10^7 PFU/ml). No plaques could be observed for the parental strain on RD cells despite high viral input multiplicities ($>10^7$ PFU/ml determined on SkMel28 cells). CVA21-DAFv induced plaques with subtle difference in phenotype on the different cell substrates; on RD cells, large (>1.5-mm), cloudy plaques were observed within 2 days postinfection whereas only uniformly small plaques (<1 mm) of high definition were observed on SkMel28 cells (Fig. 1C). The smaller plaques observed on SkMel28 cells may reflect a slightly reduced growth capacity of CVA21-DAFv in SkMel28 cells. However, 10 successive back passages of CVA21-DAFv in SkMel28 cells failed to select revertants to the parental phenotype, with the back-passaged CVA21-DAFv still retaining the capacity to lytically infect RD cells at low multiplicities of infection (data not shown). Therefore, the enhanced DAF usage of the CVA21-DAFv appears to be a stable and desirable phenotype even in the presence of high levels of ICAM-1.

CVA21-DAFv binds to the N-terminal domains of DAF and ICAM-1. The prototype strain of CVA21 binds to the N-terminal domains of both ICAM-1 and DAF (30, 43). To examine whether CVA21-DAFv binds directly to ICAM-1 and/or DAF like the prototype strain, radiolabeled binding assays were performed using CHO cells stably expressing ICAM-1 or DAF. Flow cytometric studies displayed very high levels of surface expression of DAF (GMF = 296.2) or ICAM-1 (GMF = 146.2) on the respective transfected CHO cell lines (Fig. 2A). As expected, the CVA21 parental strain bound to both ICAM-1 and DAF on transfected CHO cells (43) (Fig. 2B). Significant amounts of CVA21-DAFv bound to both CHO-DAF and CHO–ICAM-1 cells, while only background binding was observed to CHO cells (Fig. 2B). The specificities of the viral interactions with surface-expressed ICAM-1 and DAF on the transfected CHO cells were confirmed using specific anti-DAF SCR1 and anti-ICAM-1 MAb to block viral attachment (31). Such MAb blockade reduced the binding of both viruses to background levels, while an anti-DAF SCR3 MAb blockade did not reduce or enhance viral binding of either CVA21 preparation to the DAF-transfected CHO cells (Fig. 2B). The above data suggest that, like the parental strain, CVA21-DAFv binds to the N-terminal domains of ICAM-1 and DAF.

Antibody cross-linking of DAF does not enhance the cell infectivity of CVA21-DAFv. To investigate whether subtle differences, if any, exist between the CVA21 parental and CVA21-DAFv strains in the binding or usage of moderate levels of endogenously expressed DAF, radiolabeled virus-binding assays were employed to assess the relative levels of attachment to RD and DOV13 cells (ovarian carcinoma cell line). Flow cytometric analysis revealed that RD and DOV13 cells lack ICAM-1 expression but express comparable levels of DAF (GMF = 64.0 and 84.0, respectively) (Fig. 2A). Virus-binding levels were determined in both the presence and absence of surface DAF antibody cross-linking. The bioselected CVA21-DAFv exhibited significant levels of binding to both RD and DOV13 cells, while little to no attachment to these cells was observed for the parental strain (Fig. 2C). Like the

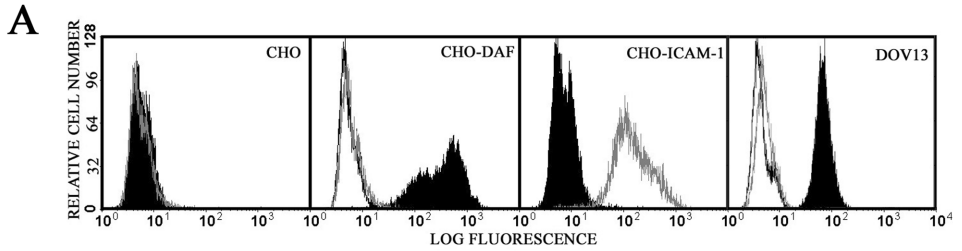
A
CHO
CHO-DAF
CHO-ICAM-1
DOV13
RELATIVE CELL NUMBER
LOG FLUORESCENCE

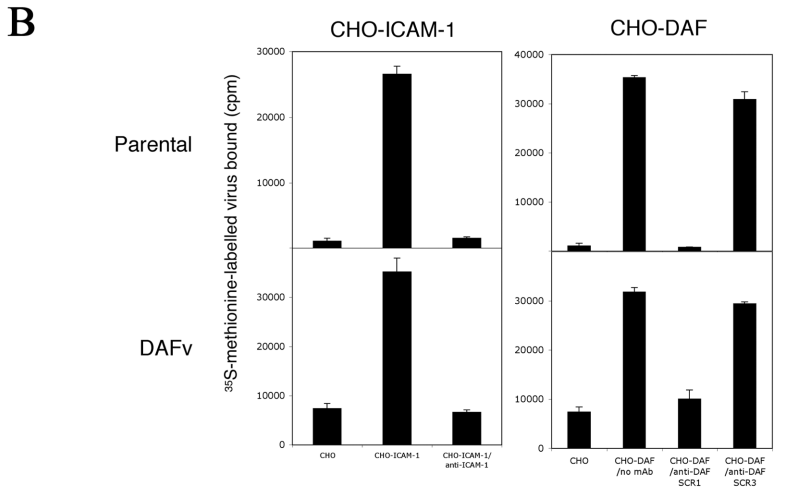
B
CHO-ICAM-1
CHO-DAF
Parental
DAFv
35S-methionine-labelled virus bound (cpm)
CHO
CHO-ICAM-1
CHO-ICAM-1/ anti-ICAM-1
CHO-DAF /no mAb
CHO-DAF /anti-DAF SCR1
CHO-DAF /anti-DAF SCR3

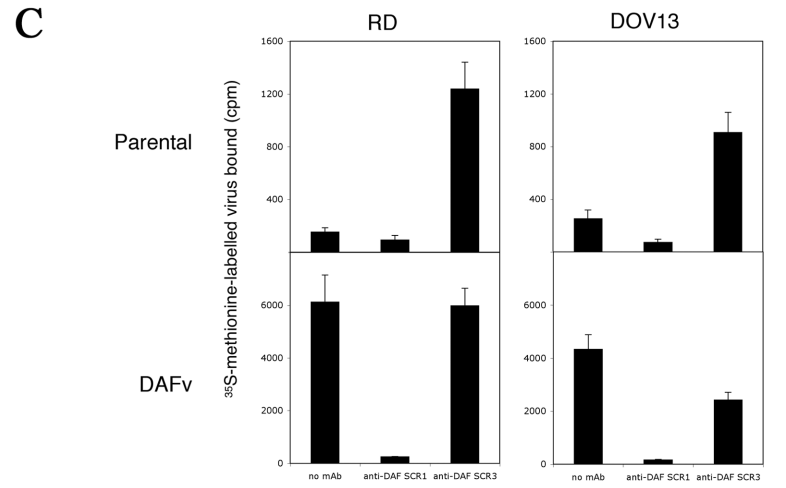
C
RD
DOV13
Parental
DAFv
35S-methionine-labelled virus bound (cpm)
no mAb
anti-DAF SCR1
anti-DAF SCR3

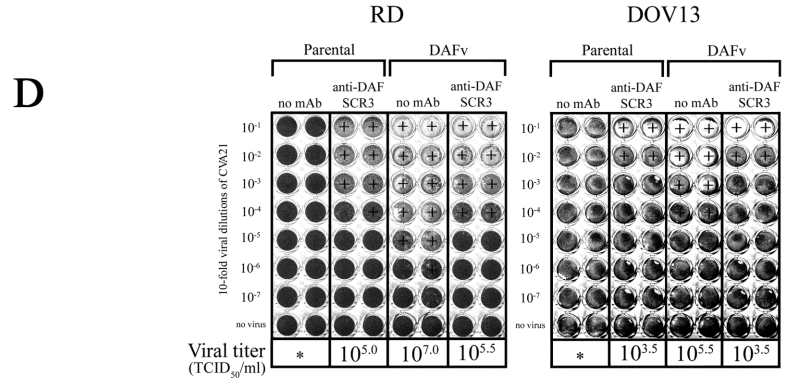
D
RD
DOV13
Parental
DAFv
no mAb
anti-DAF SCR3
10-fold viral dilutions of CVA21
no virus
Viral titer (TCID50/ml)
*
10^5.0
10^7.0
10^5.5
10^3.5
10^5.5
10^3.5

viral binding to CHO-DAF cells, specific CVA21-DAFv binding to RD and DOV13 cells was reduced to background levels by pretreatment with anti-SCR1 MAb (Fig. 2C).

Cross-linking of surface-expressed DAF with a MAb directed against the non-virus-binding SCR3 domain of DAF increases binding of the prototype CVA21 to RD cells and renders the cells susceptible to lytic infection (44). We therefore investigated whether cross-linking of surface DAF results in increased cellular binding of CVA21-DAFv, as observed for the prototype strain on RD cells (39). Anti-SCR3 pretreatment enhanced parental CVA21 viral binding eightfold on RD cells and fourfold on DOV13 cells (Fig. 2C). In the case of CVA21-DAFv, anti-DAF SCR3 pretreatment had little to no effect on enhancing the binding to either RD or DOV13 cells. In fact, a slight decrease in binding of CVA21-DAFv to DOV13 cells was observed (Fig. 2C). The capacity of CVA21-DAFv to bind at significant levels to RD and DOV13 cells in the absence of MAb-cross-linked DAF suggests that CVA21-DAFv binds more avidly to DAF than does the parental strain.

To determine whether anti-DAF SCR3 MAb pretreatment affected on the susceptibility of RD and DOV13 cells to lytic infection by either CVA21 parental or CVA21-DAFv, confluent monolayers of RD and DOV13 cells were preincubated with anti-DAF SCR3 MAb before viral challenge. Viral infections were allowed to proceed for 3 days at 37°C before the monolayers were assessed for lytic infection. In the absence of DAF cross-linking by anti-DAF SCR3 MAb, RD and DOV13 cells were both refractory to infection by the CVA21 parental strain even at high viral input multiplicities (10^6 $TCID_{50}$/well). Pretreatment with an anti-DAF SCR3 MAb rendered RD and DOV13 cells susceptible to parental CVA21 lytic infection (Fig. 2D). The CVA21-DAFv induced viral titers ($>10^{5.5}$ $TCID_{50}$/ml) in both the untreated RD and DOV13 cells. Surprisingly, anti-DAF SCR3 MAb pretreatment reduced the lytic titer of CVA21-DAFv in RD and DOV13 cells ~100-fold compared to the titers observed when no MAb was present (Fig. 2D). The CVA21-DAFv binding to the DAF-expressing cells was not enhanced by the pretreatment with the anti-DAF SCR3 MAb (Fig. 2C) and, in the case of DOV13, led to slightly reduced attachment. These findings suggest that MAb binding to DAF SCR3 may interfere with the cell entry mechanism of CVA21-DAFv bound to SCR1 of DAF.

ICAM-1, not DAF, interactions induce capsid conformational changes of CVA21-DAFv. Against the background of the increased capacity of CVA21-DAFv to bind to DAF and lytically infect ICAM-1-negative cells (Fig. 1 and 2), we compared the relative binding avidity of the parental CVA21 strain and CVA21-DAFv to surface DAF. Radiolabeled virions were bound to CHO-DAF cells for 2 h at 4°C, and, following removal of unbound virions, the cell-bound virions were eluted from the cells with increasing concentrations of a competing anti-DAF SCR1 MAb. Approximately 10-fold-higher concentrations of anti-DAF SCR1 MAb were required to displace ~70% of CVA21-DAFv virions then were required to displace parental virus from these cells (Fig. 3A). This finding suggests that, in comparison with the parental strain, a less accessible site of the CVA21-DAFv virions interacts with DAF or that CVA21-DAFv virions bind to DAF with higher affinity than does the parental strain.

DAF is postulated to function as an enteroviral concentration receptor; in general, DAF-enterovirus interactions are unable to induce the formation of detectable capsid conformational changes (30, 35, 39). To investigate whether CVA21-DAFv A-particle formation was induced by interaction with surface-expressed DAF or ICAM-1, purified 160S virions were incubated with CHO-DAF or CHO-ICAM-1 cells for 2 h at 4°C. Following removal of unbound virions, cell-bound virions were permitted to elute for 2 h at 37°C and then subjected to velocity centrifugation on 5 to 30% sucrose gradients. CVA21-DAFv virions eluted from ICAM-1 displayed a reduced sedimentation coefficient, indicating the formation of A particles, and retained little to no infectivity (data not shown), a finding similar to that observed for the CVA21 prototype strain (30, 42): Despite the enhanced DAF usage of CVA21-DAFv, CVA21-DAFv virions eluted from DAF without any detectable conformational changes (Fig. 3B) and retained a high level of infectivity (data not shown).

Blockade of DAF inhibits lytic infection of CVA21-DAFv in RD cells. Lytic-cell infection and competitive binding assays suggest an enhanced interaction between surface-expressed DAF and the CVA21-DAFv compared to the parental CVA21 strain (Fig. 2 and 3). Due to the emergence of this novel receptor-using variant virus, we investigated whether anti-DAF SCR1 MAb could block CVA21-DAFv lytic infection of RD cells. Anti-DAF SCR1 MAb provided complete protection against CVA21-DAFv-induced lytic infection of RD cells even with input multiplicities in excess of 10^6 $TCID_{50}$/well (Fig. 4A). Furthermore, pretreatment of RD cells with anti-DAF SCR1 MAb inhibited the production of progeny virus (data not shown).

To further confirm that the CVA21-DAFv virions required direct interplay with surface DAF for cell infectivity, the capacity of human recombinant sDAF to inhibit their infection of RD cells was assessed. Soluble DAF interaction with CVA21-DAFv significantly inhibited cell lytic infection but had no detectable effect on reducing infection by the phylogenetically

FIG. 2. MAb blockade of CVA21-DAFv binding and lytic infection. (A) Flow cytometric analysis of surface levels of DAF and ICAM-1 on CHO, CHO-DAF, CHO-ICAM-1, and DOV13 cells. The open histogram represents binding of conjugate only, the dotted histogram represents binding of anti-ICAM-1 MAb, and the solid histogram represents binding of anti-DAF MAb. (B) Radiolabeled viral binding to surface-expressed ICAM-1 and DAF on transfected CHO cells measured by liquid scintillation counting. Results are expressed as the mean of triplicate samples plus standard deviation. (C) Radiolabeled viral binding to endogenously expressed DAF on RD and DOV13 cells measured by liquid scintillation counting. Results are expressed as the mean of triplicate samples plus standard deviation. (D) Effect of MAb cross-linking of DAF on CVA21 lytic infection of RD and DOV13 cells. Cell monolayers in 96-well plates were preincubated with anti-DAF SCR3 MAb prior to challenge with parental CVA21 and CVA21-DAFv (10-fold viral dilutions with 10^6 to 10^0 $TCID_{50}$/well). Following incubation for 72 h at 37°C, the cell monolayers were fixed and stained with a crystal violet solution. Plus signs indicate a cytopathic effect detected by microscopic examination. Asterisks indicate a viral titer less than 10 $TCID_{50}$/ml.

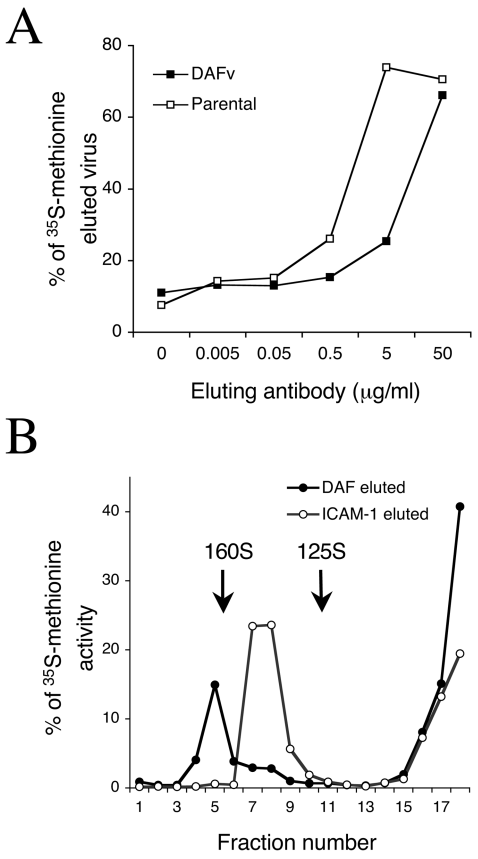

FIG. 3. Elution of CVA21-DAFv from DAF. (A) Comparison of the stringency of parental CVA21 and CVA21-DAFv binding to surface DAF. CHO-DAF cells were incubated with radiolabeled virus for 2 h at 4°C, and cell-bound virus was then eluted with different concentrations of anti-DAF SCR1 MAb (IA10) for 1 h on ice. The supernatant was monitored for the level of eluted virus, and the results are expressed as the percentage of cell-eluted radiolabeled virus. Results are expressed as the mean of duplicate samples. (B) Sedimentation of DAF- and ICAM-1-bound CVA21-DAFv virions. CHO-DAF and CHO–ICAM-1 cells were incubated with radiolabeled CVA21-DAFv virions for 2 h at 4°C, and cell-bound virus was allowed to elute for 2 h at 37°C. Sedimentation of eluted virions was analyzed on 5 to 30% sucrose gradients. Mature virions (160S) and provirions (125S) were used as internal migration controls (42).

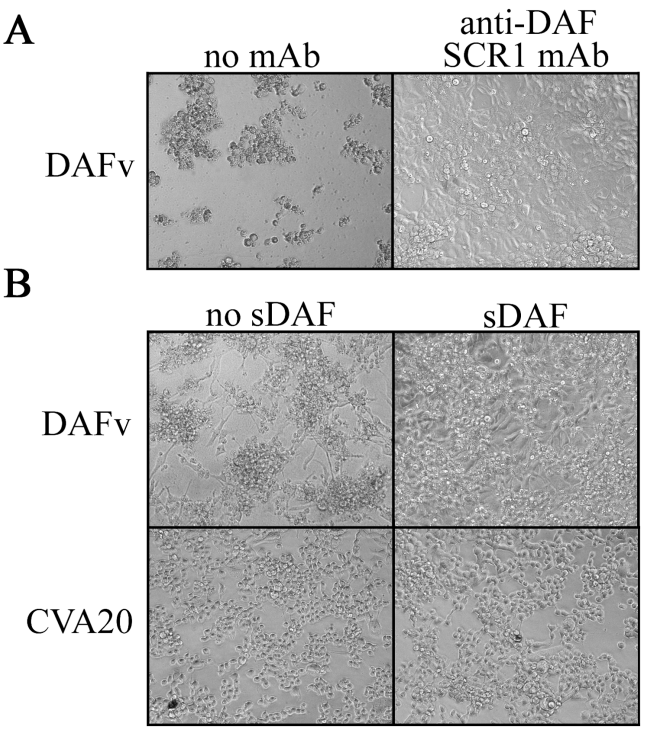

FIG. 4. Inhibition of CVA21-DAFv lytic infection by anti-DAF SCR1 MAb and sDAF. (A) Confluent monolayers of RD cells were incubated with anti-DAF SCR1 MAb IA10 prior to infection with CVA21-DAFv. Following incubation for 24 h at 37°C, the cells were inspected for cell lysis and photographed. (B) CVA21-DAFv and CVA20 (10^3 $TCID_{50}$) were incubated with sDAF (1.2 μM) for 1 h at 37°C and added to RD cell monolayers. Following incubation for 48 h at 37°C; the cells were inspected for cell lysis and photographed.

related non-DAF-binding CVA20 (Fig. 4B). Like CVA21, CVA20 binds to ICAM-1, yet it requires an unidentified receptor for cell entry (29). Overall, these findings demonstrate that CVA21-DAFv lytic infection is inhibited by anti-DAF SCR1 MAb and sDAF, confirming the crucial role of DAF interactions in the cellular entry of CVA21-DAFv.

Molecular determinants conferring the DAF phenotype of CVA21-DAFv. In an attempt to explain the expanded cell tropism and increased DAF usage phenotype of CVA21-DAFv, the nucleotide sequences of the capsid-coding region of both the CVA21 parental strain and CVA21-DAFv were determined. The capsid protein sequences were compared to that of the CVA21 Kuykendall prototype strain (29), for which the interactions with DAF and ICAM-1 have been well characterized (42, 43). Sequence analysis of the capsid-coding region of the double-plaque-purified parental strain revealed one coding substitution in VP2 (S164L) compared to the CVA21 prototype sequence (GenBank AF465515) (29). The DAF- and ICAM-1-binding properties of the CVA21 parental strain (Fig. 1 and 2) were not altered with respect to the prototype strain (43) by this VP2 amino acid substitution. Following bioselection in RD cells, the VP2 L164 residue remained in the CVA21-DAFv, while two additional amino acid substitutions were detected in VP3 (R96H and E101A) and one silent mutation was detected in VP2 (V209). As the VP2 L164 amino acid substitution is shared between the parental strain and CVA21-DAFv, it is unlikely to be involved in conferring the enhanced DAF-binding phenotype of CVA21-DAFv. CVA21-DAFv exhibited a mixed population (C/A) at nucleotide position 2038 (VP3 101), resulting in Ala/Glu, while only A (Glu) was encoded by the parental CVA21 at this position.

Since the molecular structure of CVA21 has not been determined at atomic resolution, we modeled the architecture of the parental CVA21 based on similarities to previously determined structures of related picornaviruses in an attempt to offer an explanation for the differences in DAF binding between parental CVA21 and CVA21-DAFv. The mutations possibly conferring the enhanced DAF-binding phenotype of CVA21-DAFv (VP3 R96H and E101A) are predicted to be embedded at the interface of capsid proteins VP1, VP2, and VP3 (Fig. 5). The VP3 residues R96 and E101 are covered by

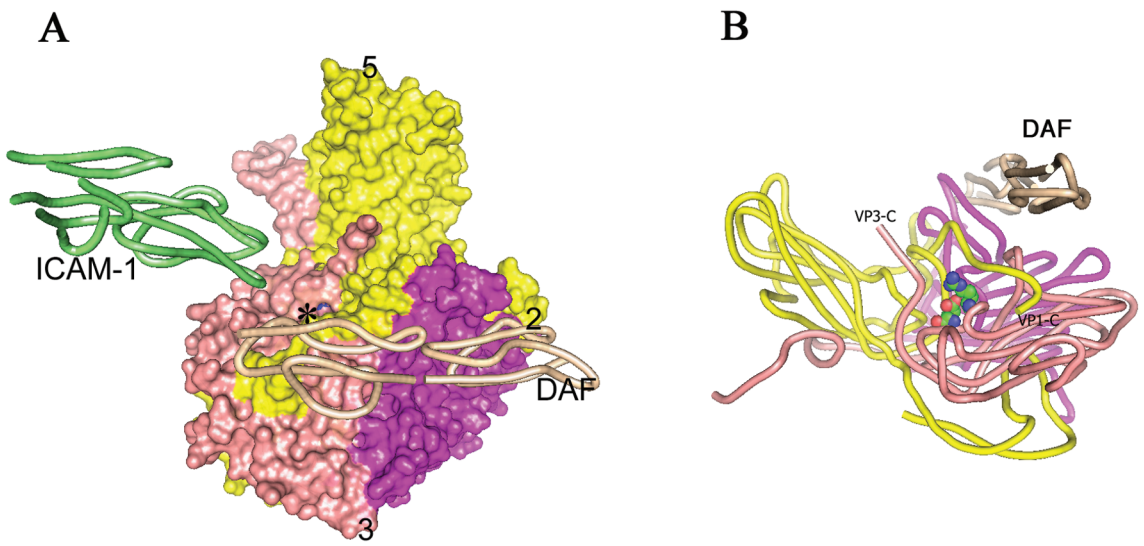

FIG. 5. Close-up view of the predicted receptor-virus-binding surface of CVA21. (A). Top view of one CVA21 protomer presented as an isosurface where VP1 is depicted in yellow, VP2 is depicted in pink, and VP3 is depicted in magenta. Numbers indicates the corresponding positions of icosahedaral five-, three-, and two-fold axes. The interacting ICAM-1 and DAF molecules are shown as worm drawings, with DAF in beige and the canyon-binding ICAM-1 in green. The position of the VP3 R96 residue in CVA21 parental (space-filling mode) is partially covered by the VP1 C-terminal loop, and only one nitrogen atom (blue surface next to the asterisk) in the arginine side chain can be viewed from the viral surface. (B) Side view of the CVA21 protomer with proteins colored as above and VP3 residues R96 and E101 highlighted in space-filling mode. VP1-C and VP3-C denote the C-terminal end of VP1 and VP3, respectively. The figure was generated with pymol software (http://www.pymol.org).

the VP3 C terminus on the side and the VP1 C terminus on the top, with only the side chain nitrogen atom of arginine (R96) being solvent accessible (blue sphere in Fig. 5A). The CVA21-DAFv attachment to DAF is postulated to occur outside the capsid canyon, as is the case for EV12 (7). While the CVA21-DAFv VP3 H96 and A101 mutations are not directly located in the proposed EV12-DAF-binding site, their positioning may impart an enhanced conformation or accessibility to the DAF-binding footprint, resulting in an increased binding affinity to DAF compared to that of the parental strain (Fig. 3A).

DISCUSSION

As it does for many other enteroviruses, DAF serves as an attachment receptor for the prototype strain of CVA21, although ICAM-1 is required for productive CVA21 infection (43). In this paper we describe a variant of CVA21 bioselected in vitro in ICAM-1-negative cells, which has acquired an altered and expanded cell tropism (Fig. 1 and 2). Radiolabeled virus-binding assays described herein indicate that despite multiple passages in ICAM-1-negative RD cells, CVA21-DAFv retained the capacity to independently bind to either the N-terminal domain of ICAM-1 or DAF SCR1 (Fig. 2). In environments of extremely high levels of surface-expressed DAF (i.e., CHO-DAF cells selected for maximal level of expression), both parental and CVA21-DAFv bound to DAF at similar levels, while only the CVA21-DAFv attached to RD and DOV13 cells which exhibited significantly less surface expression of endogenous DAF. In accordance with a previous study (44), MAb cross-linking of DAF by an anti-DAF SCR3 MAb significantly increased the binding of the parental CVA21 to DAF-expressing RD and DOV13 cells and facilitated lytic infection in the absence of ICAM-1 (Fig. 2). However, no increase in viral binding or lytic infection by the CVA21-DAFv to MAb cross-linked RD or DOV13 cells was observed. This finding suggests that, in comparison with the parental strain, the bioselected CVA21-DAFv has optimized its interactions with DAF and that such interactions are not further enhanced by MAb cross-linking of DAF. The data indicating that parental CVA21 virions are more easily displaced than CVA21-DAFv from surface-expressed DAF during incubation with an epitope competing anti-DAF SCR1 MAb further support the postulate of an enhanced DAF-binding phenotype of the CVA21-DAFv compared to the parental strain (Fig. 3).

It is postulated that the role of DAF for the CVA21 prototype strain is to hold the virus in an infectious state, awaiting interactions with the entry receptor, ICAM-1, and direct binding to DAF alone does not initiate productive infection by the CVA21 prototype strain (30, 43). Despite the high level of surface expression of DAF or ICAM-1 on the surface of transfected CHO cells (Fig. 2A), no detectable cell infection by the parental CVA21 or CVA21-DAFv could be observed (data not shown). However, evidence in support of the enhanced DAF usage by the CVA21-DAFv is supplied by the lytic infection of ICAM-1-negative RD and DOV13 cells, which can be completely blocked by anti-DAF SCR1 MAb blockade alone even at high viral inputs (Fig. 4). This is in contrast to the partial block caused by the same MAb for the CVA21 prototype strain when used in a multiple-receptor environment of DAF and ICAM-1 coexpression, where MAbs against both DAF and ICAM-1 are required to totally block infection (43). These findings support the postulate that CVA21-DAFv employs surface DAF as a functional cellular receptor. The observation that infection by CVA21-DAFv was inhibited by sDAF at concentrations comparable to those previously shown to have an inhibitory effect on enteroviral infections (35) further high-

lights the importance of the role of DAF in CVA21-DAFv infection of RD cells (Fig. 4). Additionally, it provides evidence against the possibility that during the bioselection process, the CVA21-DAFv has adapted to use another, unidentified, secondary cellular receptor involved in cellular internalization in the absence of ICAM-1. The enhanced DAF-binding phenotype of CVA21-DAFv compared to that of the parental CVA21 (Fig. 2 and 3) appears to be translated into increased cellular lytic infection (Fig. 2), not only in RD cells but also in DAF-expressing ovarian cancer cells (DOV13).

There are numerous discrete differences in the binding interactions of many human enteroviruses to DAF. The DAF-binding sites on the CVB3, EV7, and EV12 virions are postulated to be located outside the capsid canyon at the icosahedral twofold symmetry axes (7, 14, 27). While EV11 also interacts with DAF outside the canyon region, the DAF-binding footprint is postulated to be located near the fivefold axes of the virion (47). Of the human enteroviruses that attach to DAF, only enterovirus 70 and CVA21 bind to the N-terminal SCR1 domain of DAF (19, 30); the remaining DAF-binding enteroviruses interact with the central domains (SCR2–4) (9, 23, 36). In addition to the fact that enterovirus binding to DAF is located outside the canyon, these interactions are reported not to result in cell infection or formation of A-particles (30, 35, 45). In the case of EV11, for which DAF binding has been assessed quantitatively, interactions with DAF are of low affinity, as opposed to the interactions of the canyon-binding ICAM-1 molecule to rhinovirus 3, which is of similar affinity but of slower kinetics (23).

Although CVA21-DAFv is exhibiting an enhanced DAF-binding phenotype, only two amino acids in the capsid-coding region differ from those in the parental strain. During the bioselection process, CVA21-DAFv retained the capacity to bind ICAM-1 (Fig. 2). Therefore, not surprisingly, none of the observed capsid mutations were located in the previously determined ICAM-1-binding footprint, which is postulated to span the north and south canyon rims (49). The observed mutations of CVA21-DAFv are predicted to be located outside the capsid canyon in the VP3 α-helix (CD loop) surrounded by the VP2 EF loop and the C termini of VP1 and VP3 (Fig. 5). The two mutations are predicted to be in close contact with the C termini of VP1 and VP3 via interactions with VP1 R270 and VP3 H329. It is proposed that the observed mutations in CVA21-DAFv VP3 may be involved in enhancing the conformation of the VP3 α-helix and the C-terminal region of VP1, which corresponds to the DAF binding footprint on the surface of EV12 (7). Such conformational changes would result in better contact between the CVA21-DAFv capsid and DAF. The postulate of an increased affinity between DAF and the twofold depression of CVA21-DAFv virions due to the presence of VP3 H96 and A101 is in agreement with the finding that it is more difficult to displace CVA21-DAFv than parental virions from surface-expressed DAF by challenge with an anti-DAF SCR1 MAb (Fig. 3A). Low-passage clinical isolates of CVA21, which, to various degrees, can lytically infect DAF-expressing RD cells in the absence of MAb cross-linking of DAF and ICAM-1 expression, also encode VP3 H96 but not the A101 mutation observed in CVA21-DAFv (31). In comparison, the prototype CVA21 strain encodes VP3 R96. The presence of VP3 H96, the more surface-exposed residue of the two herein-observed mutations, in the clinical CVA21 isolates and in CVA21-DAFv is thus suggested to be a crucial residue in conferring the enhanced DAF usage and subsequent pathogenesis of CVA21. Although not addressed in this study, the involvement of additional mutations outside the capsid-coding region in mediating cell lytic infection cannot be excluded. However, the enhanced capacity of radiolabeled CVA21-DAFv virions to attach to surface DAF reflects mutations within the capsid-coding region rather than involvement of other viral genomic regions.

Cross-linked DAF-mediated cell lytic infection by the prototype CVA21 occurs at a lower rate than that mediated via ICAM-1 interactions, with the cell entry suggested to occur via different entry mechanisms (39). The cross-linked DAF-mediated entry of prototype CVA21 occurs without detectable A-particle formation and is postulated to involve caveolae (39), a novel entry route recently implicated in the entry of EV1 and a DAF-binding strain of EV11 (26, 46). Attachment of EV1 to its receptor $\alpha_2\beta_1$ on the cell surface results in integrin clustering (51) and is suggested to facilitate viral entry in a similar manner to that for prototype CVA21-mediated entry via cross-linked DAF (39). Following MAb cross-linking, DAF is postulated to be presented in a more favorable conformation on the cell surface, thereby rendering cells susceptible to infection by the prototype CVA21 (39). Binding of the CVA21-DAFv to surface DAF appears to occur in the absence of detectable formation of A particles (Fig. 3B). A possible explanation for this finding is that in a similar fashion to that previously postulated for low-passage clinical CVA21 isolates (also possessing the VP3 H96 residue [31]), the CVA21-DAFv virions can effectively cross-link DAF and thereby gain entry into the cell by a mechanism related to the artificial action of cross-linking MAb. The apparent lack of detectable CVA21-DAFv A particles eluted from the cell surface does not prove that no A particles are being formed. A particles will fail to accumulate if the subsequent uncoating events occur faster than the initial DAF-mediated conversion of 160S to 135S particles (17). EV1, which uses the $\alpha_2\beta_1$-integrin for cell entry (6), binds to the functional α_2I domain of the $\alpha_2\beta_1$-integrin in the capsid canyon (51). Despite being a classical canyon-binding receptor, the EV1 interaction with α_2I does not result in viral uncoating (51), in contrast to binding of the soluble forms of the poliovirus receptor to poliovirus and ICAM-1 to rhinovirus (1, 16, 50). Interaction between $\alpha_2\beta_1$-integrin-expressing cells and EV1 has, however, been implied to mediate conformational changes of the virion, but it remains uncertain whether additional cellular molecules are required for EV1 uncoating (26, 51). In a similar manner, it cannot be ruled out that an additional cellular protein(s) is required for CVA21-DAFv uncoating or that the presence of the mutations in the viral capsid may destabilize the capsid and thereby evade the need for a receptor-mediated conformational change.

The capacity of CVA21-DAFv to lytically infect two cancerous cell lines of different phenotypes and tissue origins (RD and DOV13) highlights the fact that the acquired use of DAF as a functional receptor is not restricted to the particular cellular substrate used in the bioselection process. The expression of DAF and other complement-regulatory proteins is enhanced on the surface of many tumor cells of different origins relative to normal cells to protect the cells from the comple-

ment-mediated attack (18, 24, 28). It is suggested that CVA21-DAFv-mediated oncolysis via specific capsid interactions with surface-expressed DAF, due to the enhanced DAF-binding phenotype, could potentially be effective in the control of some human malignancies. In support of this strategy is the successful application of the prototype strain of CVA21, which is effective in the control of melanoma tumors, targeted via ICAM-1 and DAF, which both are overexpressed on the surface of malignant melanoma cells (40). A major finding of the present study is that viral bioselection may be a viable alternative to direct genetic manipulation in the development of novel tumor-targeting oncolytic enteroviruses.

ACKNOWLEDGMENTS

We thank Bruce Loveland, Taroh Kinoshita, Andrew Boyd, Margery Kennett, S. J. Ralph, and Ian Campbell for the generous gifts that made this study possible; Linda Berry, Leone Beagly, Gough Au, and Dianne Sylvester for excellent technical assistance; and Richard Barry for many helpful discussions.

This research was supported by grants from the National Health and Medical Research Council of Australia and Hunter Medical Research Institute. E.S.J was supported by a postdoctoral scholarship from the Swedish Research Council.

REFERENCES

1. **Arita, M., S. Koike, J. Aoki, H. Horie, and A. Nomoto.** 1998. Interaction of poliovirus with its purified receptor and conformational alteration in the virion. J. Virol. **72:**3578–3586.
2. **Belnap, D. M., D. J. Filman, B. L. Trus, N. Cheng, F. P. Booy, J. F. Conway, S. Curry, C. N. Hiremath, S. K. Tsang, A. C. Steven, and J. M. Hogle.** 2000. Molecular tectonic model of virus structural transitions: the putative cell entry states of poliovirus. J. Virol. **74:**1342–1354.
3. **Belnap, D. M., B. M. McDermott, Jr., D. J. Filman, N. Cheng, B. L. Trus, H. J. Zuccola, V. R. Racaniello, J. M. Hogle, and A. C. Steven.** 2000. Three-dimensional structure of poliovirus receptor bound to poliovirus. Proc. Natl. Acad. Sci. USA **97:**73–78.
4. **Bergelson, J. M., M. Chan, K. R. Solomon, N. F. St. John, H. Lin, and R. W. Finberg.** 1994. Decay-accelerating factor (CD55), a glycosylphosphatidylinositol-anchored complement regulatory protein, is a receptor for several echoviruses. Proc. Natl. Acad. Sci. USA **91:**6245–6248.
5. **Bergelson, J. M., J. A. Cunningham, G. Droguett, E. A. Kurt-Jones, A. Krithivas, J. S. Hong, M. S. Horwitz, R. L. Crowell, and R. W. Finberg.** 1997. Isolation of a common receptor for coxsackie B viruses and adenoviruses 2 and 5. Science **275:**1320–1323.
6. **Bergelson, J. M., M. P. Shepley, B. M. C. Chan, M. E. Hemler, and R. W. Finberg.** 1992. Identification of the integrin VLA-2 as a receptor for echovirus 1. Science **255:**1718–1720.
7. **Bhella, D., I. G. Goodfellow, P. Roversi, D. Pettigrew, Y. Chaudhry, D. J. Evans, and S. M. Lea.** 2003. The structure of echovirus type 12 bound to a two-domain fragment of its cellular attachment protein decay-accelerating factor (CD 55). J. Biol. Chem. **279:**8325–8332.
8. **Boyd, A. W., S. O. Wawryk, G. F. Burns, and J. V. Fecondo.** 1988. Intercellular adhesion molecule 1 (ICAM-1) has a central role in cell-cell contact-mediated immune mechanisms. Proc. Natl. Acad. Sci. USA **85:**3095–3099.
9. **Clarkson, N. A., R. Kaufman, D. M. Lublin, T. Ward, P. A. Pipkin, P. D. Minor, D. J. Evans, and J. W. Almond.** 1995. Characterization of the echovirus 7 receptor: domains of CD55 critical for virus binding. J. Virol. **69:**5497–5501.
10. **Colonno, R. J., J. H. Condra, S. Mizutani, P. L. Callahan, M. E. Davies, and M. A. Murcko.** 1988. Evidence for the direct involvement of the rhinovirus canyon in receptor binding. Proc. Natl. Acad. Sci. USA **85:**5449–5453.
11. **Coyne, K. E., S. E. Hall, S. Thompson, M. A. Arce, T. Kinoshita, T. Fujita, D. J. Anstee, W. Rosse, and D. M. Lublin.** 1992. Mapping of epitopes, glycosylation sites, and complement regulatory domains in human decay accelerating factor. J. Immunol. **149:**2906–2913.
12. **He, Y., V. D. Bowman, S. Mueller, C. M. Bator, J. Bella, X. Peng, T. S. Baker, E. Wimmer, R. J. Kuhn, and M. G. Rossmann.** 2000. Interaction of the poliovirus receptor with poliovirus. Proc. Natl. Acad. Sci. USA **97:**79–84.
13. **He, Y., P. R. Chipman, J. Howitt, C. M. Bator, M. A. Whitt, T. S. Baker, R. J. Kuhn, C. W. Anderson, P. Freimuth, and M. G. Rossmann.** 2001. Interaction of coxsackievirus B3 with the full length coxsackievirus-adenovirus receptor. Nat. Struct. Biol. **8:**874–878.
14. **He, Y., F. Lin, P. R. Chipman, C. M. Bator, T. S. Baker, M. Shoham, R. J. Kuhn, M. E. Medof, and M. G. Rossmann.** 2002. Structure of decay-accelerating factor bound to echovirus 7: a virus-receptor complex. Proc. Natl. Acad. Sci. USA **99:**10325–10329.
15. **He, Y., S. Mueller, P. R. Chipman, C. M. Bator, X. Peng, V. D. Bowman, S. Mukhopadhyay, E. Wimmer, R. J. Kuhn, and M. G. Rossmann.** 2003. Complexes of poliovirus serotypes with their common cellular receptor, CD155. J. Virol. **77:**4827–4835.
16. **Hoover-Litty, H., and J. M. Greve.** 1993. Formation of rhinovirus-soluble ICAM-1 complexes and conformational changes in the virion. J. Virol. **67:**390–397.
17. **Huang, Y., J. M. Hogle, and M. Chow.** 2000. Is the 135S poliovirus particle an intermediate during cell entry? J. Virol. **74:**8757–8761.
18. **Juhl, H., F. Helmig, K. Baltzer, H. Kalthoff, D. Henne-Bruns, and B. Kremer.** 1997. Frequent expression of complement resistance factors CD46, CD55, and CD59 on gastrointestinal cancer cells limits the therapeutic potential of monoclonal antibody 17–1A. J. Surg. Oncol. **64:**222–230.
19. **Karnauchow, T. M., S. Dawe, D. M. Lublin, and K. Dimock.** 1998. Short consensus repeat domain 1 of decay-accelerating factor is required for enterovirus 70 binding. J. Virol. **72:**9380–9383.
20. **Karnauchow, T. M., D. L. Tolson, B. A. Harrison, E. Altman, D. M. Lublin, and K. Dimock.** 1996. The HeLa cell receptor for enterovirus 70 is decay-accelerating factor (CD55). J. Virol. **70:**5143–5152.
21. **Kinoshita, T., M. E. Medof, R. Silber, and V. Nussenzweig.** 1985. Distribution of decay-accelerating factor in the peripheral blood of normal individuals and patients with paroxysmal nocturnal hemoglobinuria. J. Exp. Med. **162:**75–92.
22. **Kolatkar, P. R., J. Bella, N. H. Olson, C. M. Bator, T. S. Baker, and M. G. Rossmann.** 1999. Structural studies of two rhinovirus serotypes complexed with fragments of their cellular receptor. EMBO J. **18:**6249–6259.
23. **Lea, S. M., R. M. Powell, T. McKee, D. J. Evans, D. Brown, D. I. Stuart, and P. A. van der Merwe.** 1998. Determination of the affinity and kinetic constants for the interaction between the human virus echovirus 11 and its cellular receptor, CD55. J. Biol. Chem. **273:**30443–30447.
24. **Li, L., I. Spendlove, J. Morgan, and L. G. Durrant.** 2001. CD55 is overexpressed in the tumour environment. Br. J. Cancer **84:**80–86.
25. **Lukacik, P., P. Roversi, J. White, D. Esser, G. P. Smith, J. Billington, P. A. Williams, P. M. Rudd, M. R. Wormald, D. J. Harvey, M. D. Crispin, C. M. Radcliffe, R. A. Dwek, D. J. Evans, B. P. Morgan, R. A. Smith, and S. M. Lea.** 2004. Complement regulation at the molecular level: the structure of decay-accelerating factor. Proc. Natl. Acad. Sci. USA **101:**1279–1284.
26. **Marjomäki, V., V. Pietiäinen, H. Matilainen, P. Upla, J. Ivaska, L. Nissinen, H. Reunanen, P. Huttunen, T. Hyypiä, and J. Heino.** 2002. Internalization of echovirus 1 in caveolae. J. Virol. **76:**1856–1865.
27. **Muckelbauer, J. K., M. Kremer, I. Minor, G. Diana, F. J. Dutko, J. Groarke, D. C. Pevear, and M. G. Rossmann.** 1995. The structure of coxsackievirus B3 at 3.5 Å resolution. Structure **3:**653–667.
28. **Murray, K. P., S. Mathure, R. Kaul, S. Khan, L. F. Carson, L. B. Twiggs, M. G. Martens, and A. Kaul.** 2000. Expression of complement regulatory proteins-CD 35, CD 46, CD 55, and CD 59-in benign and malignant endometrial tissue. Gynecol. Oncol. **76:**176–182.
29. **Newcombe, N. G., P. Andersson, E. S. Johansson, G. G. Au, A. M. Lindberg, R. D. Barry, and D. R. Shafren.** 2003. Cellular receptor interactions of C-cluster human group A coxsackieviruses. J. Gen. Virol. **84:**3041–3050.
30. **Newcombe, N. G., L. G. Beagley, D. Christansen, B. E. Loveland, E. S. Johansson, K. W. Beagley, R. D. Barry, and D. R. Shafren.** 2004. Novel role for decay-accelerating factor in coxsackievirus A21-mediated cell infectivity. J. Virol. **78:**12677–12682.
31. **Newcombe, N. G., E. S. Johansson, G. Au, A. M. Lindberg, R. D. Barry, and D. R. Shafren.** 2004. Enteroviral capsid interactions with decay-accelerating factor mediate lytic cell infection. J. Virol. **78:**1431–1439.
32. **Pallansch, M. A., and R. P. Roos.** 2001. Enteroviruses: polioviruses, coxsackieviruses, echoviruses and newer enteroviruses, p. 723–776. *In* D. M. Knipe, P. M. Howley, D. E. Griffin, R. A. Lamb, M. A. Matrin, B. Roizman, and S. E. Straus (ed.), Fields virology, 4th ed, vol. 1. Lippincott Williams & Wilkins, Philadelphia, Pa.
33. **Pearson, W. R., and D. J. Lipman.** 1988. Improved tools for biological sequence comparison. Proc. Natl. Acad. Sci. USA **85:**2444–2448.
34. **Powell, R. M., V. Schmitt, T. Ward, I. Goodfellow, D. J. Evans, and J. W. Almond.** 1998. Characterization of echoviruses that bind decay accelerating factor (CD55): evidence that some haemagglutinating strains use more than one cellular receptor. J. Gen. Virol. **79:**1707–1713.
35. **Powell, R. M., T. Ward, D. J. Evans, and J. W. Almond.** 1997. Interaction between echovirus 7 and its receptor, decay-accelerating factor (CD55): evidence for a secondary cellular factor in A-particle formation. J. Virol. **71:**9306–9312.
36. **Powell, R. M., T. Ward, I. Goodfellow, J. W. Almond, and D. J. Evans.** 1999. Mapping the binding domains on decay accelerating factor (DAF) for haemagglutinating enteroviruses: implications for the evolution of a DAF-binding phenotype. J. Gen. Virol. **80:**3145–3152.
37. **Reed, L. J., and H. A. Muench.** 1938. A simple method of estimating fifty per cent endpoints. Am. J. Hyg. **27:**493–497.
38. **Sali, A., and T. L. Blundell.** 1993. Comparative protein modelling by satisfaction of spatial restraints. J. Mol. Biol. **234:**779–815.
39. **Shafren, D. R.** 1998. Viral cell entry induced by cross-linked decay-accelerating factor. J. Virol. **72:**9407–9412.

40. **Shafren, D. R., G. G. Au, T. Nguyen, N. G. Newcombe, E. S. Haley, L. Beagley, E. S. Johansson, P. Hersey, and R. D. Barry.** 2004. Systemic therapy of malignant human melanoma tumors by a common cold producing enterovirus: coxsackievirus A21. Clin. Cancer Res. **10:**53–60.
41. **Shafren, D. R., R. C. Bates, M. V. Agrez, R. L. Herd, G. F. Burns, and R. D. Barry.** 1995. Coxsackieviruses B1, B3, and B5 use decay-accelerating factor as a receptor for cell attachment. J. Virol. **69:**3873–3877.
42. **Shafren, D. R., D. J. Dorahy, S. J. Greive, G. F. Burns, and R. D. Barry.** 1997. Mouse cells expressing human intercellular adhesion molecule-1 are susceptible to infection by coxsackievirus A21. J. Virol. **71:**785–789.
43. **Shafren, D. R., D. J. Dorahy, R. A. Ingham, G. F. Burns, and R. D. Barry.** 1997. Coxsackievirus A21 binds to decay-accelerating factor but requires intercellular adhesion molecule 1 for cell entry. J. Virol. **71:**4736–4743.
44. **Shafren, D. R., D. J. Dorahy, R. F. Thorne, T. Kinoshita, R. D. Barry, and G. F. Burns.** 1998. Antibody binding to individual short consensus repeats of decay-accelerating factor enhances enterovirus cell attachment and infectivity. J. Immunol. **160:**2318–2323.
45. **Shafren, D. R., D. T. Williams, and R. D. Barry.** 1997. A decay-accelerating factor-binding strain of coxsackievirus B3 requires the coxsackie-adenovirus receptor protein to mediate lytic infection of rhabdomyosarcoma cells. J. Virol. **71:**9844–9848.
46. **Stuart, A. D., H. E. Eustace, T. A. McKee, and T. D. Brown.** 2002. A novel cell entry pathway for a DAF-using human enterovirus is dependent on lipid rafts. J. Virol. **76:**9307–9322.
47. **Stuart, A. D., T. A. McKee, P. A. Williams, C. Harley, S. Shen, D. I. Stuart, T. D. Brown, and S. M. Lea.** 2002. Determination of the structure of a decay-accelerating factor-binding clinical isolate of echovirus 11 allows mapping of mutants with altered receptor requirements for infection. J. Virol. **76:**7694–7704.
48. **Ward, T., P. A. Pipkin, N. A. Clarkson, D. M. Stone, P. D. Minor, and J. W. Almond.** 1994. Decay-accelerating factor CD55 is identified as the receptor for echovirus 7 using CELICS, a rapid immuno-focal cloning method. EMBO J. **13:**5070–5074.
49. **Xiao, C., C. M. Bator, V. D. Bowman, E. Reider, Y. He, B. Hébert, J. Bella, T. S. Baker, E. Wimmer, R. J. Kuhn, and M. G. Rossmann.** 2001. Interaction of coxsackievirus A21 with its cellular receptor, ICAM-1. J. Virol. **75:**2444–2451.
50. **Xing, L., J. M. Casasnovas, and R. H. Cheng.** 2003. Structural analysis of human rhinovirus complexed with ICAM-1 reveals the dynamics of receptor-mediated virus uncoating. J. Virol. **77:**6101–6107.
51. **Xing, L., M. Huhtala, V. Pietiäinen, J. Kapyla, K. Vuorinen, V. Marjomäki, J. Heino, M. S. Johnson, T. Hyypiä, and R. H. Cheng.** 2003. Structural and functional analysis of integrin alpha21 domain interaction with echovirus 1. J. Biol. Chem. **279:**11632–11638.
52. **Xing, L., K. Tjarnlund, B. Lindqvist, G. G. Kaplan, D. Feigelstock, R. H. Cheng, and J. M. Casasnovas.** 2000. Distinct cellular receptor interactions in poliovirus and rhinovirus. EMBO J. **19:**1207–1216.